Imaging melanin cancer growth in-vivo using raster-scan optoacoustic mesoscopy (RSOM) at 50 MHz and 100 MHz

Murad Omar*[a+], Mathias Schwarz[a+], Dominik Soliman[a], Panagiotis Symvoulidis[a], and Vasilis Ntziachristos[a]

[a]Institute for Biological and Medical Imaging, TU Muenchen and Helmholtz Zentrum Muenchen, Ingolstaedter Landstr. 1, 85764, Neuherberg, Germany

ABSTRACT

We used raster-scan optoacoustic mesoscopy (RSOM) at 50 MHz, and at 100 MHz, to monitor tumor growth, and tumor angiogenesis, which is a central hallmark of cancer, *in-vivo*. In this study we compared the performance, and the effect of the 50 MHz, and the 100 MHz frequencies on the quality of the final image.

The system is based on a reflection-mode implementation of RSOM. The detectors used are custom made, ultrawideband, and spherically focused. The use of such detectors enables light coupling from the same side as the detector, thus reflection-mode. Light is in turn coupled using a fiber bundle, and the detector is raster scanned in the xy-plane. Subsequently, to retrieve small features, the raw data are reconstructed using a multi-bandwidth, beamforming reconstruction algorithm.

Comparison of the system performance at the different frequencies shows as expected a higher resolution in case of the 100 MHz detector compared to the 50 MHz. On the other hand the 50 MHz has a better *SNR*, can detect features from deeper layers, and has higher angular acceptance. Based on these characteristics the 50 MHz detector was mostly used.

After comparing the performance we monitored the growth of B16F10 cells, melanin tumor, over the course of 9 days. We see correspondence between the optoacoustic measurements and the cryoslice validations. Additionally, in areas close to the tumor we see sprouting of new vessels, starting at day 4-5, which corresponds to tumor angiogenesis.

Keywords: Optoacoustics, high frequency, beam-forming, epi-illumination, mesoscopy, microscopy

1. INTRODUCTION

Optoacoustics is a relatively new imaging modality, which overcomes the limitations of optical imaging by indirectly measuring the generated ultrasound. The advantages of this over a pure optical method is that you directly get absorption, and the scattering of ultrasonic waves is 2-3 orders of magnitude lower in biological tissue than it is for optical waves[1]. Because of these characteristics optoacoustics has been growing recently, and it has been used for macroscopic applications[2-4], mesoscopic[5, 6], and microscopic ones[7-9]. In the tomographic case the achieved resolutions are on the order of 100-200 μm, and the depth of imaging is 1-2 cm, thus such approaches are useful for whole body small animal imaging[4], or for clinical applications[10]. The advantages over other modalities in this case are the high resolution imaging, combined with high depth of penetration, and the delivery of functional and molecular parametrs of disease biomarkers.

*murad.omar@tum.de; www.cbi.ei.tum.de

+These authors contributed equally to this work.

Photons Plus Ultrasound: Imaging and Sensing 2016, edited by Alexander A. Oraevsky, Lihong V. Wang
Proc. of SPIE Vol. 9708, 97080S · © 2016 SPIE · CCC code: 1605-7422/16/$18 · doi: 10.1117/12.2209298

On the other hand optoacoustic microscopy uses focused beams of light to image the tissue[7, 9, 11], this can achieve micrometer resolution on the order of 1-2 µm, but at only superficial depths of 500 µm maximum, limited by the optical diffusion of tissue[1]. The advantages of such a method over conventional optical microscopic techniques are the delivery of functional parameters of the tissue such as metabolism, and tissue oxygenation in a label free manner and at microscopic resolutions. Additionally it gives information about tissue absorption in a reflection mode, which is not possible to measure by other modalities.

Because the resolution achieved by optoacoustic tomographic or macroscopic methods is on the order of 100-200 µm it is essentially useless to image a sample smaller than 5 mm in diameter. Thus, a gap exists between what microscopic techniques can do, and when tomographic technique become efficient, we call this gap the mesoscopic gap. To image in this gap we propose the use of high frequency ultrasound detectors in the range of 50-100 MHz, additionally instead of imaging only in the focus we synthetically focus the data outside the focus using synthetic focusing, and beamforming algorithms, this allows high resolution imaging even at depths of several millimeters, depending on the absorption and scattering of the sample being investigated.

In a previous work we introduced raster-scan optoacoustics mesoscopy (RSOM) both in transmission and reflection mode[6, 12]. Herein based on the reflection mode implementation we study the suitability of RSOM for imaging of neovascularization in a tumor model of melanin[13]; we show the suitability of RSOM for imaging the neovascularization in tumors, as well as a comparison between RSOM at 50 MHz, and at 100 MHz for the imaging of cancer, and angiogenesis which is a central hallmark of cancer[14].

2. METHODS

2.1 Hardware

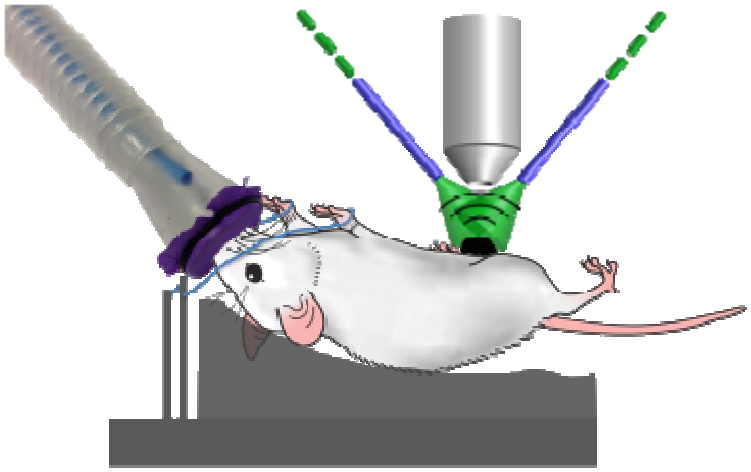

Fig. 1: experimental setup. The mouse is fixed on an ergonomic bed, an anaesthesia mask is on the mouse. The scan head consisting of the detector and the fiber bundles scan the region of the tumor.

The system consists of two custom made, high-frequency ultrasound detectors, with a center frequency of 100 MHz and 50 MHz respectively, the system is called RSOM100 when used with the 100 MHz detector, and RSOM50 when used with the 50 MHz detector. The bandwidth of RSOM100 is 20-180 MHz, the detector has a diameter of 1.5 mm, and an f_{number} of ~1.1. On the other hand the bandwidth of RSOM50 is 10-90 MHz, the detector has a diameter of 3 mm, and an f_{number} of ~0.98.

The excitation happens through a fiber bundle with 3 arms, which couples the light. The fiber bundle is connected from one side to a fast diode pumped solid state laser (DPSS) (Wedge HB532, BrightSolutions, Italy), operating at 532 nm, which although doesn't penetrate deep, increases contrast from the upper layers, which are the interesting ones for high-resolution, microscopic and mesoscopic applications. On the other side the fiber bundle is connected to a scanning head, and illuminate the sample from three directions. In the middle of the scan head the ultrasound detector is located. The output of the ultrasound detector is connected to a low noise amplifier, with an amplification of 63 dB, and a bandwidth of 0.001-500 MHz (AU-1291, Miteq Inc. USA), this is subsequently connected to a high speed data acquisition card, operating at 900 MSps for RSOM100, and at 450 MSps for RSOM50

(ADQ412-3G, SP Devices, Sweden). The signals are initially filtered in the 20-180 MHz or in the 10-90 MHz range depending on the detector used to reject noise from outside of the detection bandwidth.

Finally, The detector is positioned on two piezo stages for fast scanning of the samples. The stages are operated in a discrete continuous manner for faster scanning.

2.2 Reconstruction and multi-bandwidth signal processing

From theoretical analysis, and simulations, it could already be confirmed that under wide illumination the small objects will generate weaker signals than larger objects will. This could be factored into two reasons; the first of which is attenuation, where the high frequencies experience a stronger attenuation than low frequencies do[15], for example in biological tissue the attenuation increases linearly with the frequency. The second factor is the efficiency of generation, where under thermal and stress confinement conditions the amplitude of the generated optoacoustic signal is linearly proportional to the diameter of the object. Thus, all in all the *SNR* of small objects is much weaker than the *SNR* of larger objects. Hence, to correctly represent both the high and the low frequencies on the same image we proposed to use a multi-bandwidth approach[6], where the low frequencies are reconstructed separately from the high frequencies, and eventually the images, the high frequency, and the low frequency are overlayed using different colors. In this paper we use the same approach but we estimate the bandwidths differently[13]. Here instead of dividing the total bandwidth into two equal bandwidths, we divide it into two bandwidths with equivalent relative bandwidth ($BW_{\%}$):

$$\frac{BW_1}{f_{c1}} = \frac{BW_2}{f_{c2}} = \frac{BW_3}{f_{c3}} = \cdots \quad (1)$$

Using the above relationship can help us determine the following cutoff frequency as:

$$f_2 = \frac{2+BW_{\%}}{2-BW_{\%}} f_1. \quad (2)$$

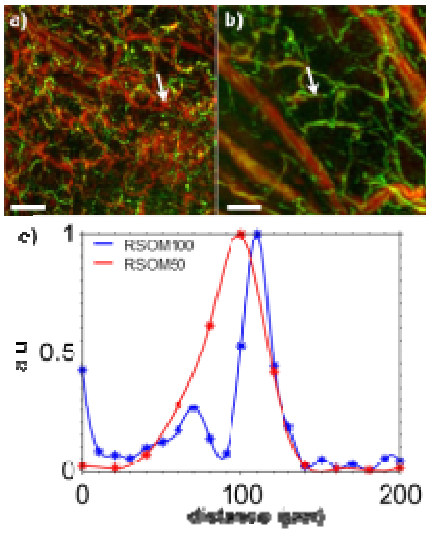

Fig. 2: a) an image taken with RSOM100, b) an image taken with RSOM50, c) profiles from RSOM100 and RSOM50 across the vessel pinpointed by the arrows in a) and b). Scale bars: 500 µm.

The filtering is done using an exponential bandpass filter of the fourth order. Furthermore the reconstruction is performed using a GPU parallelized beamforming algorithm with a dynamic aperture to account for the spatial characteristics of the detectors used[6].

2.3 Tumor imaging

For tumor imaging we used a mouse model of melanin cancer, where B16F10 cells were orthotopically injected into the mouse. Two days after the injection we started imaging over a total period of 9 days. The imaging was performed both with RSOM100 and RSOM50[13]. The animals were anaesthetized during the experiments, and all the animal handling was performed according to the approved animal protocol of the government of upper Bavaria.

At the start we compared the performance of RSOM100 and RSOM50 in imaging tumors, later we used RSOM50 to follow the tumor growth over time.

2.4 Validation and cryoslice imaging

After the final imaging point the animals were sacrificed and cryosliced, the cryoslicing was performed the same way as reported by Symvoulidis et al[16]. The cryoslices were used for validation and for comparison with the optoacoustic images.

3. RESULTS

3.1 Comparison between RSOM100 and RSOM50

The mice were imaged both in RSOM100 and RSOM50. The main points of comparison between the two systems were imaging speed, resolution, and quality of the generated images. For a field of view of 12 × 12 mm^2 the acquisition takes around 12 minutes and 3 minutes respectively, the reason behind this discrepancy is that the step size required for RSOM100 is smaller than the one required for RSOM50; 10 µm and 20 µm respectively. The resolution of both the systems is determined by the diffraction limited acoustic focusing of the ultrasound detector used. Based on the measurements of the tumor itself we could find vessels as small as 20 µm and 42.5 µm, which is close to the theoretically predictable resolution of both the systems[13], see Fig.2.
Finally, the quality of the vessels imaged using RSOM100 in comparison to the ones imaged using RSOM50 was evaluated depending on the signal to noise ratio (*SNR*) of the generated images, as well as the completeness of the vessel structures imaged in both cases. From the generated images the *SNR* of RSOM100 is slightly worse than that of RSOM50, more importantly because of the wider angle of acceptance of the 50 MHz detector the vessels look much more continuous in comparison to RSOM100.

3.2 Imaging of tumor development

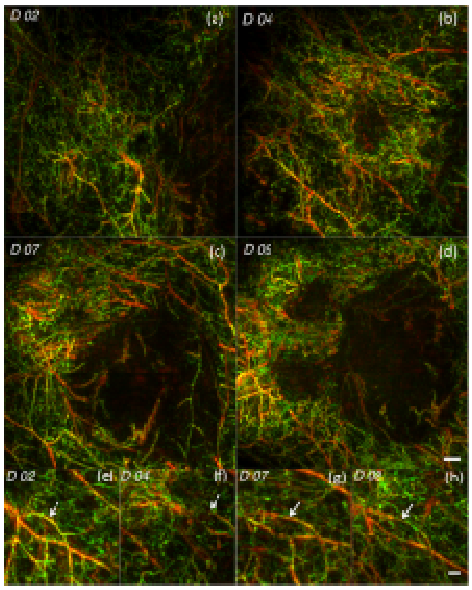

Fig. 3: a)-d) Follow up on tumor growth using RSOM, e)-h) a zoom in on a region close to the tumor which shows the increase in neovascularization. Scale bars: d)1 mm, h) 0.5 mm

Because of the faster acquisition time, as well as the better quality of images generated from RSOM50 we used it for monitoring the tumor development. Longitudinal imaging was done over the course of 9 days, on day 2, day 4, day 7, and day 9 after injection. After imaging and reconstruction we looked for prominent vessels, or structures on the images to monitor the growth. On the observed images we see three things, a redistribution of the vessels due to tumor growth, the tumor growth, and the generation of neovascularization, which becomes prominent after day 4. The neovascularization could be observed because we used multi-bandwidth reconstruction.

4. SUMMARY & DISCUSSION

We have shown in this work the suitability of RSOM for cancer imaging, we also shown some of the trade-offs between using 50 MHz and 100 MHz in imaging of tumor development. Generally RSOM100 will image smaller vessels, and give better resolution, nonetheless, these comes at the expense of time and signal to noise ratio. Additionally we have seen the importance of the angle of acceptance of the detector on the total quality of the images, where it gives better quality of the images, and improves the visibility of the elongated structures, such as the vessels in the case of tumor growth.

We foresee RSOM to play a vital role in further studies of neovascularization, and cancer research. The use of RSOM allows imaging of vasculature at depths beyond what microscopy or OCT can do[17], with good resolution, and fast acquisition times.

In a manner similar to skin imaging[18, 19], to further advance the system multispectral imaging is of interest[20], multispectral information will fuse the anatomical information from the tumor itself with functional and molecular information, for a better understanding of the tumor biology, and it's growth. Additionally, advancements in optical

detectors will enable the manufacturing of point like detectors, with wide angular acceptance, and a flat bandwidth[21, 22]. Another addition might be using a hybrid optoacoustic ultrasound to collect even more information about the anatomy, and the heterogeneity of the tumor[23, 24].

REFERENCES

1. Ntziachristos, V., *Going deeper than microscopy: the optical imaging frontier in biology.* Nature Methods, 2010. **7**(8): p. 603-614.
2. Beziere, N. and V. Ntziachristos, *Optoacoustic imaging: an emerging modality for the gastrointestinal tract.* Gastroenterology, 2011. **141**(6): p. 1979-85.
3. E. Herzog, et al., *Optical imaging of cancer heterogeneity with multispectral optoacoustic tomography.* Radiology, 2012. **263**(2): p. 461-468.
4. V. Ntziachristos and D. Razansky, *Molecular imaging by means of Multispectral optoacoustic tomography (MSOT).* Chemical Reviews, 2010. **110**(5): p. 2783-2794.
5. Chekkoury, A., et al., *Optical mesoscopy without the scatter: broadband multispectral optoacoustic mesoscopy.* Biomedical Optics Express, 2015. **6**(9): p. 3134-3148.
6. Omar, M., et al., *Ultrawideband reflection-mode optoacoustic mesoscopy.* Optics Letters, 2014. **39**(13): p. 3911-3914.
7. Soliman, D., et al., *Combining microscopy with mesoscopy using optical and optoacoustic label-free modes.* Scientific reports, 2015. **5**.
8. J. Yao and L.V. Wang, *Photoacoustic microscopy.* Laser & Photonics Reviews, 2013. **7**(5): p. 758-778.
9. Yao, J. and L.V. Wang, *Sensitivity of photoacoustic microscopy.* Photoacoustics, 2014. **2**(2): p. 87-101.
10. Deán-Ben, X.L. and D. Razansky, *Adding fifth dimension to optoacoustic imaging: volumetric time-resolved spectrally enriched tomography.* Light: Science & Applications, 2014. **3**(1): p. e137.
11. G.J. Tserevelakis, et al., *Hybrid Multi-photon and Optoacoustic Microscope.* Optics Letters, 2014. **39**.
12. Omar, M., J. Gateau, and V. Ntziachristos, *Raster-scan optoacoustic mesoscopy in the 25-125 MHz range.* Opt Lett, 2013. **38**(14): p. 2472-4.
13. Omar, M., et al., *Pushing the Optical Imaging Limits of Cancer with Multi-Frequency-Band Raster-Scan Optoacoustic Mesoscopy (RSOM).* Neoplasia, 2015. **17**(2): p. 208-214.
14. Hanahan, D. and R.A. Weinberg, *Hallmarks of cancer: the next generation.* Cell, 2011. **144**(5): p. 646-674.
15. Dean-Ben, X.L., D. Razansky, and V. Ntziachristos, *The effects of acoustic attenuation in optoacoustic signals.* Phys Med Biol, 2011. **56**(18): p. 6129-48.
16. Symvoulidis, P., et al. *Serial sectioning and multispectral imaging system for versatile biomedical applications*. in *Biomedical Imaging (ISBI), 2014 IEEE 11th International Symposium on*. 2014. IEEE.
17. Vakoc, B.J., et al., *Three-dimensional microscopy of the tumor microenvironment in vivo using optical frequency domain imaging.* Nature medicine, 2009. **15**(10): p. 1219-1223.
18. Aguirre;, J., et al., *Broadband mesoscopic optoacoustic tomography reveals skin layers.* Optics Letters, 2014. **39**(21): p. 6297-6300.

19. M. Schwarz, et al., *Implications of ultrasound frequency in optoacoustic mesoscopy of the skin.* IEEE transactions on medical imaging, 2015. **34**(2): p. 672-677.
20. Schwarz, M., et al., *Three-dimensional multispectral optoacoustic mesoscopy reveals melanin and blood oxygenation in human skin in vivo.* Journal of biophotonics, 2015. **9**(1-2): p. 55-60.
21. Rosenthal, A., et al., *Embedded ultrasound sensor in a silicon-on-insulator photonic platform.* Applied Physics Letters, 2014. **104**(2): p. 021116.
22. Rosenthal, A., et al., *Sensitive interferometric detection of ultrasound for minimally invasive clinical imaging applications.* Laser & Photonics Reviews, 2014. **8**(3): p. 450-457.
23. Subochev, P., et al., *Simultaneous photoacoustic and optically mediated ultrasound microscopy: an in vivo study.* Biomedical optics express, 2015. **6**(2): p. 631-638.
24. Estrada, H., et al., *Hybrid optoacoustic and ultrasound biomicroscopy monitors' laser-induced tissue modifications and magnetite nanoparticle impregnation.* Laser Physics Letters, 2014. **11**(12): p. 125601.